Cavity ring-down spectroscopy

Martyn D. Wheeler, Stuart M. Newman, Andrew J. Orr-Ewing† and Michael N. R. Ashfold School of Chemistry, University of Bristol, Cantock's Close, Bristol, UK BS8 1TS

FARADAY RESEARCH ARTICLE

Cavity ring-down spectroscopy (CRDS) is a laser-based absorption spectroscopy technique that is starting to find extensive application as a consequence of the very high sensitivity of the method compared with more traditional absorption spectroscopy techniques. We describe the experimental implementation of CRDS and its application to a number of areas of research including laser diagnostics of hostile environments, reaction kinetics and spectroscopy, with particular emphasis on our ongoing studies of the fast (sub-nanosecond) predissociation of electronically excited states of small molecules and radicals.

1 Introduction

In recent years a new, ultra-sensitive laser absorption spectroscopy technique has been developed,1 evolving from previous techniques used, for example, to measure mirror reflectivities.^{2,3} The technique is most widely known as cavity ring-down spectroscopy (CRDS), although the alternative, but more cumbersome, cavity ring-down laser absorption spectroscopy (CRLAS) is preferred by some authors. The CRDS technique is a direct absorption spectroscopy that has numerous advantages compared with traditional absorption techniques: in particular, CRDS is largely immune to shot-to-shot variations in the laser intensity, and benefits from tremendously long effective pathlengths (up to tens of kilometres) through a sample using a bench-top apparatus. The consequences are that CRDS exhibits very high sensitivity, sufficient, for example, for trace detection of radical species in the troposphere. In addition, the high resolution of the tunable lasers used for CRDS make it a versatile and general tool for studies of molecular spectroscopy and dynamics. The generality of the technique stems from the single requirement that the molecule or radical absorb electromagnetic radiation generated by a laser (provided that the high-reflectivity mirrors needed for CRDS can be obtained in the wavelength region of the absorption). It is fairly simple to implement experimentally but, until recently, progress has been hampered by the lack of commercially available, ultra-high reflectivity mirrors required for the experiments. As an illustration of the sensitivity of CRDS, in Fig. 1 we show a spectrum of the electric-dipole forbidden b $^1\Sigma_{\rm g}^{}-X\,^3\Sigma_{\rm g}^{}$ (2, 0) transition in molecular oxygen. This transition is driven by a (much weaker) magnetic-dipole interaction, and the (2, 0) band has a Franck–Condon factor ca. 300 times smaller than that of the (0, 0) band. The spectrum shown was taken in a 1.5 m long cell containing 750 Torr of O_2 .

In this article, we outline the background, implementation, and applications of CRDS. We illustrate the generality of the technique by describing some key studies that make use of the resolution and sensitivity of the method. In particular, we concentrate on a review of our ongoing studies of molecular predissociation. First, however, we outline the basics of absorption spectroscopy and consider alternative, high-sensitivity laser methods commonly employed for laser spectroscopy and diagnostics so that we can draw comparisons with the CRDS method. This overview of laser methods is only cursory because of the extensive existing literature. 4.5 We also address what we regard as the primary limitations of CRDS and discuss likely future developments in the experimental methods that will extend the versatility of the technique.

† e-mail: a.orr-ewing@bristol.ac.uk

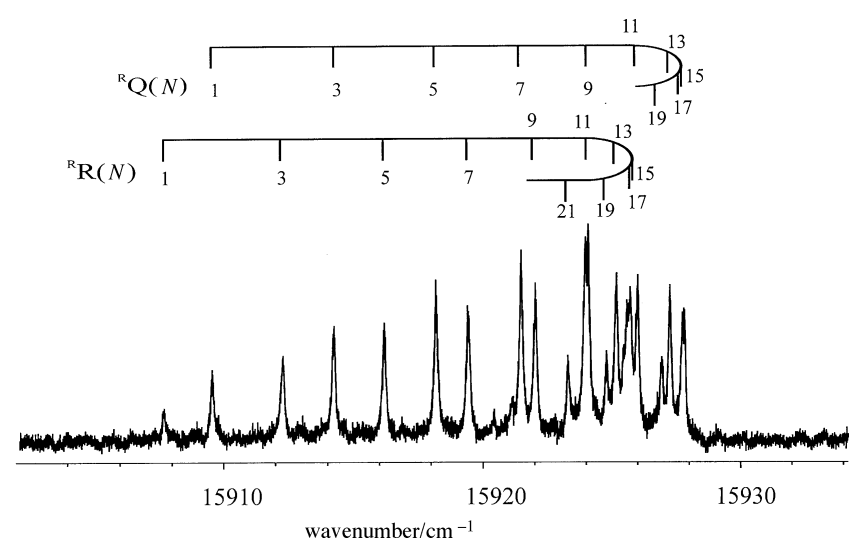


Fig. 1 CRD spectrum of the electric-dipole forbidden O_2 b ${}^1\Sigma_g{}^+$ – X ${}^3\Sigma_g{}^-$ (2,0) transition, recorded using 750 Torr of O_2 in a 1.5 m cavity. The rotational line assignments are indicated by the combs above the spectrum.

1.1 Absorption spectroscopy, the Beer-Lambert law

The absorption and emission of electromagnetic (EM) radiation by atoms or molecules are the key physical processes used in spectroscopic analysis. The absorption of light by a sample is described by the Beer–Lambert⁶ law which gives a quantitative relationship between the intensity of a spectral feature and the frequency-dependent absorption properties of the sample:

$$I = I_0 \exp[-\sigma Cl] \tag{1}$$

Here, I_0 and I are the intensities of light entering and leaving the sample, respectively, C is the concentration of the absorber, l is the sample pathlength and σ is the absorption cross-section of the sample at the particular wavelength of the light. The product of C and σ is the absorption coefficient, α , and the absorbance is defined as σCl .

Conventional (non-laser) implementations of absorption spectroscopy require broad-band or continuum light sources, with the wavelength dependence of absorption obtained by dispersing the light that exits the sample through a monochromator. To achieve high resolution, narrow monochromator slits must be used and the light is dispersed over a large distance (of the order of metres) before reaching the detector (traditionally a photographic plate, but more recently a diode array or CCD camera), thereby decreasing the throughput. The inherent non-linearities in detection of light using photographic plates make quantitative interpretation of spectral lineshapes and linewidths unreliable. Using tunable laser sources, however, it is possible to record absorption spectra by detecting the change in intensity of the beam emerging from the sample as the laser wavelength is varied. The sensitivity of any absorption technique is ultimately governed by the pathlength of the beam through the sample, and thus the sensitivity may be increased by using a multiple-pass (e.g. White cell) arrangement, e.g. 50 traversals of a 20 cm cell results in an effective pathlength of 10 m.

The main problem with laser absorption spectroscopy when detecting inherently weak absorptions (e.g. trace gas detection, or electric-dipole forbidden but magnetic-dipole allowed transitions such as the O₂ b $^1\Sigma_{\rm g}{}^+-{\rm X}\,^3\Sigma_{\rm g}{}^-$ system) is that the change in intensity of the light as it passes through the sample is very small compared with the initial laser intensity, so the sensitivity is generally limited by fluctuations in I_0 . However, several other laser-based methods of obtaining absorption-like spectra exist which rely upon some subsequent side effect of the excitation process; some examples of such methods are briefly outlined below.

1.2 Laser induced fluorescence (LIF)

Following the absorption of a photon of light, an electronically excited molecule may decay to its ground state by emission of radiation, a process known as fluorescence. By monitoring this fluorescence (generally at 90° to the laser beam) molecular absorption can be detected as the input laser wavelength is scanned.8 LIF is, at least in theory, a zerobackground technique, but some sources of noise are inevitable, the principal one usually being scattered laser light from optical surfaces. LIF is thus a highly sensitive absorption technique: for example, for detection of tropospheric OH, a sensitivity of 1.8 × 10⁶ molecules cm⁻³ was recently demonstrated and further improvements have since been made.⁹ Detection of fluorescence is ultimately constrained by the quantum efficiency of the photomultiplier tube (PMT). A primary limitation of LIF is the requirement that the excited state have a large fluorescence quantum yield. Many excited electronic states decay via other competing pathways, such as predissociation or collisional quenching, and thus show little or no fluorescence: we shall illustrate the effect of predissociation on

the LIF signal later in this article. LIF is generally restricted to excitation wavelengths in the visible and UV regions of the electromagnetic spectrum since fluorescence rates are much slower at longer wavelengths. Examples of small molecules and radicals commonly probed by LIF include I₂, NO, OH, CH, CN, NO₂ and CO.

1.3 Resonance enhanced multiphoton ionisation (REMPI)

A molecule can be induced to absorb two or more photons simultaneously provided the intensity of light is sufficiently high to compensate for the very small cross-sections for such processes. Typically, small molecules composed of light atoms will have ionisation energies around 10-15 eV,10 corresponding to the absorption of three UV photons from the ground state of the neutral molecule. The cross-section of this ionisation process is greatly enhanced if there is a real excited state resonant at the energy of one or two absorbed photons. By monitoring the photoionisation yield as the laser is scanned, a spectrum corresponding to absorption to the resonant state is obtained.11-13 REMPI has certain advantages over single photon spectroscopy; in particular, different selection rules for multiphoton transitions allow many previously unobservable transitions to be seen (e.g. for the two-photon absorption, $g \rightarrow g$ and $u \rightarrow u$ transitions in a centrosymmetric molecule), and it can be mass selective if used in combination with timeof-flight (TOF) detection. If the resonant state is heavily predissociated, however, little or no ion formation will occur. Key species detected by REMPI include H₂, HCl, NO and CH₃.

1.4 Photoacoustic spectroscopy

Absorption of EM radiation raises the internal energy of the molecules in a sample. This energy can be dissipated to a bath gas via collisions that cause internal (e.g. electronic or vibrational) to translational (E \rightarrow T or V \rightarrow T) energy transfer, resulting in a local, thermally induced pressure increase. A pulsed laser or modulated cw laser will thus generate pressure waves when tuned to be resonant with an absorption feature of the sample gas, and these pressure waves may be monitored by a piezoelectric detector or a microphone placed within the sample cell. The intensity of the sound detected depends on the degree of heating, which, in turn, is related to the strength of the absorption: hence, plotting sound level versus laser frequency yields an absorption spectrum.¹⁴ Photoacoustic spectroscopy is a highly sensitive form of laser absorption spectroscopy: for example, Davidson et al.15 specified a limiting absorption coefficient of 4×10^{-10} cm⁻¹. The technique has thus found extensive applications in the study of high vibrational overtones of small hydride molecules.

1.5 Degenerate four-wave mixing (DFWM)

DFWM involves the interaction of three coherent laser beams of identical frequencies with a medium to produce a fourth, coherent signal beam. 16-19 A simple, qualitative description of the process is as follows: two laser beams cross at a small angle to produce an optical fringe pattern, which, in an absorbing medium, will give rise to a spatial modulation of ground and excited state populations. The third laser beam can then be scattered by Bragg diffraction from the population grating to produce a signal beam. This process happens when the medium absorbs; therefore, detection of the signal beam gives an absorption spectrum. DFWM has the advantage over LIF and REMPI that it can be used to detect rapidly predissociating species without resultant loss of signal. Because of its coherent nature, the signal beam may be detected remotely, making DFWM a useful probe of hostile environments such as flames and plasmas. However, in practice, DFWM is a difficult technique to implement and the extraction of quantum-state population distributions from the resultant spectra is complicated by the non-linear nature of the interaction of light and matter in the DFWM process. DFWM signal intensities scale with the square of the concentration of the detected species, making detection of trace species very difficult, and DFWM cannot generally be regarded as possessing the sensitivity of either LIF or REMPI. Nevertheless, it has been used for the successful detection of, for example, HCO from the photolysis of acetaldehyde, ²⁰ CH in a flame ²¹ and both C₂ and CH in a diamond-growth reactor. ²²

1.6 Intracavity laser absorption spectroscopy (ICLAS)

An absorber placed within a laser cavity can alter the gain and hence the output of the laser. Therefore, by placing a narrow band absorber into the cavity of a laser and determining the gain at different wavelengths, an absorption spectrum can be obtained. The wavelength-dependent gain can be determined either by tuning the (narrow-band) laser or by using a broad-band multimode laser and dispersing the output light with a high resolution spectrograph. Quantitative intensity measurements may be extracted from these spectra, allowing concentrations or oscillator strengths to be determined. ICLAS is a very sensitive technique which may be performed in the visible using a dye laser or in the IR using a colourcentre laser, and has been applied to a number of species to measure high overtone spectra²³ and absolute concentrations, such as for HCO in a methane–air flame.²⁴

2 Experimental principles of CRDS

2.1 Cavity ring-down apparatus

A schematic diagram of the apparatus used for CRDS studies, such as those performed in our group, is shown in Fig. 2. The particular details of our experimental apparatus have been described in detail elsewhere. 25,26 The ring-down cavity (RDC) itself consists of an absorption cell bounded by highreflectivity (HR), dielectric-coated, concave mirrors which either act as vacuum chamber windows, or are located within the vacuum chamber. Mirror coatings are chosen so as to perform with maximum reflectivity (typically >99.9%) over the wavelength range of interest. The range of wavelengths spanned by any particular set of HR mirrors depends on the wavelength, the nature of the coating, and the manufacturer, but in our experience a few tens of nanometres is typical. The mirrors used are concave with radii of curvature appropriate to the establishment of a stable cavity configuration.²⁷ The output from a tunable laser source is steered so as to be aligned along the cavity axis determined by the two mirrors.

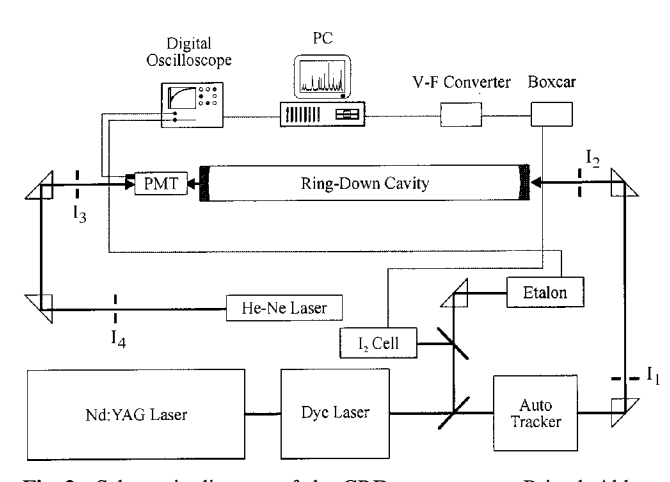


Fig. 2 Schematic diagram of the CRD apparatus at Bristol. Abbreviations in the figure are: photomultiplier tube (PMT), voltage-to-frequency converter (V-F) and irises (I) used to assist cavity alignment. The iodine cell and etalon provide accurate calibration of the laser wavelength.

The majority of experiments to date have used pulsed lasers, but applications with cw lasers are becoming more commonplace (as will be discussed later). Most of the laser light is reflected directly back from the input mirror, but a small fraction (typically $\leq 0.1\%$, depending on the reflectivity) is coupled into the cavity by transmission through the mirror. The mirrors are mounted in such a way that their positions can be minutely adjusted by use of micrometer screws, and with careful alignment it is possible to trap a laser pulse inside the cavity by ensuring it retroreflects back and forth between the mirrors. A pulse may be stored for microseconds in the RDC, corresponding to thousands of round trips, before decaying away because of cavity losses. These losses reduce the intensity of the trapped light pulse by a given percentage on each round trip.

A photo-sensitive detector and light-collection optics are positioned behind the output mirror to record the intensity of the light pulse transmitted through the mirror on each roundtrip of the cavity. If the laser pulses are shorter in temporal duration than the round-trip time of the cavity, a sufficiently fast detector will observe discrete pulses at the output mirror as some fraction of light intensity is transmitted on each trip. The train of intensity spikes will exhibit an exponential decay envelope, as shown in Fig. 3, because of the constant fractional loss of light at each mirror surface. The pulse train is, however, generally smoothed into an exponential decay by the time response of the detection electronics. The signal from the detector (usually a PMT, or fast photodiode) is amplified and digitised; a computer is then used to fit the digital trace to a first-order exponential function in order to determine the decay time constant for each laser pulse. Measuring the ringdown decay time rather than the total light intensity exiting the cavity removes from the final spectrum any shot-to-shot fluctuations in pulse intensity because the decay time constant is independent of the laser intensity. This, and the high sensitivity that stems from the extremely long (tens of kilometres for very high quality mirrors) pathlengths that may be achieved, enables the detection of absorptions smaller than one part in 107 per pass (see Section 4).28 CRDS is thus a powerful technique particularly suited to the spectroscopy of very weak transitions, or of molecules present at very low concentrations.

The exponential decay envelope time constant is determined by the cavity length, mirror reflectivity and the attenuation of the laser pulse by any absorbing medium in the cavity, as discussed in more detail in Section 2.2. If the laser is scanned in frequency, with the sample of interest held inside

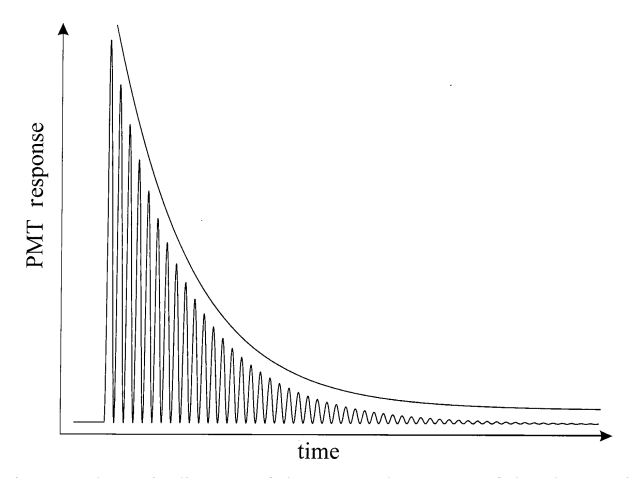


Fig. 3 Schematic diagram of the expected response of the photomultiplier tube to a train of laser pulses leaking through one cavity end mirror after successive cavity round trips. Also shown is the exponential envelope arising from smoothing of the pulse train by the time response of the experimental detection apparatus.

the cavity, absorption by the sample causes more rapid decay of the light intensity. Thus, the variation of the decay time constant with frequency produces a spectrum with absolute absorbances at those frequencies at which the laser is tuned into resonance with a molecular transition.

2.2 Obtaining a cavity ring-down spectrum

Traditional absorption spectroscopy measurements determine the attenuation of a light beam passed through a sample and measure absorption coefficients from the ratio of intensities of the light exiting and entering the sample container via the Beer-Lambert law [eqn. (1)]. As such, these methods must measure a small change in a large intensity and hence require very stable light sources with small intensity fluctuations over time. The approach used in a CRDS experiment differs because the quantity determined experimentally is the rate of decay of the light intensity within the cavity, and hence CRDS is much less sensitive to variations in the laser pulse intensity. In this Section we discuss the form of the decay of the light intensity, and how absorbances and absorption coefficients can be extracted from the decay rate. A discussion of the possible complications of cavity modes is deferred to Section 3. Careful consideration of cavity mode effects is important because the sample cell used in the CRDS apparatus is bounded by two high reflectivity mirrors without intervening surfaces and, just as in an etalon, the separation of the two fixed mirrors determines the structure and frequency spacing of the cavity modes for light trapped within the cavity. The mode structure of a cavity, its consequences for cavity ringdown spectroscopy, and the influence of laser bandwidth have been discussed at length by several authors, notably Zalicki and Zare,²⁸ Lehmann and Romanini,²⁹ and Hodges et al.,30,31 and have been reviewed by Scherer et al.32 We will therefore restrict ourselves to a summary of the conclusions of these analyses and will indicate the conditions appropriate for recording CRDS spectra with accurate spectral intensities and without omitting any spectral features.

As a first consideration of the behaviour of the light within the cavity, we will ignore the effects of cavity modes and consider just the decay of the intensity of the light within the cavity at a particular wavelength. For an empty cavity bounded by two mirrors of reflectivity R, separated by a distance l, the light intensity exiting the cavity will decay with an exponential time profile (or envelope for pulsed light, as discussed in the previous Section) according to:³³

$$I(t) = I_0 \exp\{-t/\tau\} \tag{2}$$

Here, $\tau = l/c \mid \ln R \mid \approx l/c(1-R)$ is the empty cavity ring-down time (RDT), the time for the intensity to decay to 1/e of its original value. Cavity losses by mirror transmission and other processes, such as diffraction and scattering, are equal to 1-R. The empty cavity RDT is thus determined by these loss processes, and depends strongly on the reflectivity of the mirrors. For a cavity bounded by two mirrors of reflectivity R, the number of round trips, N, performed in the time taken for the intensity to fall to 1/e of its initial value is obtained by solving $R^{2N} = 1/e$, or $N = -1/[2 \ln(R)]$. Thus, for example, for a mirror reflectivity of 0.999, N = 500, whereas for R = 0.999 99, N = 50 000, giving a pathlength in a 1 m cavity of 100 km. The extreme sensitivity of CRDS is, in part, a consequence of these very long pathlengths for the probe light through a sample.

If the wavelength of the light within the cavity matches an absorption of a sample gas held between the mirrors, the additional mechanism for loss of light from the cavity by sample absorption speeds up the decay of the trapped light intensity. For absorption conditions corresponding to Beer–Lambert law behaviour, the decay of the light intensity will still be

exponential, with time dependence given by:33

$$I(t) = I_0 \exp\left\{-\frac{t}{\tau} - \alpha ct\right\} \tag{3}$$

Here α is the molecular absorption coefficient (with dimensions of length⁻¹, and generally quoted in cm⁻¹) and c is the speed of light [not the concentration as in eqn. (1)]. The product of c and t is the pathlength, L, over which the absorption is measured. The decay rate is now given by $1/\tau' = 1/\tau + c\alpha$. We will discuss briefly the conditions under which eqn. (3) applies later in this article.

If the empty cavity RDT, τ , is known, measurement of the decay rate of the light intensity as the wavelength of the laser is scanned gives the absorption coefficient for each laser wavelength, and hence the absorption spectrum. For a discrete spectrum, τ can be determined from the baseline level between absorption features (where $\alpha=0$). Note that the quantity obtained is the absorption coefficient (or absorbance) and thus a knowledge of the partial pressure of the absorbing species within the cavity is required to extract absorption cross-sections. Two simple methods for extracting spectra from the exponential decays recorded at each laser wavelength are as follows.

- (i) Direct fitting (e.g. least-squares fitting) of the exponential decay or of its logarithm. The time region of the exponential fitted determines the effective pathlength through the sample. The fit will give the decay time τ' .
- (ii) Setting two gates of equal width on the exponential at some time separation Δt . This time separation then determines the pathlength, and the signal is measured as:³³

$$S = \ln \left\{ \frac{S_{A}}{S_{B}} \right\} = -\frac{\Delta t}{\tau} - L\alpha \tag{4}$$

where S_A and S_B are the signals measured in the first and second time gates. Clearly this manipulation of S_A and S_B gives a value that is directly proportional to the absorption coefficient.

Both methods rely on the decay being a true exponential in order to extract accurate α values. As Hudgens³⁴ has pointed out, care must be taken in any averaging procedure as it is mathematically incorrect to average out shot-to-shot fluctuations by adding a series of exponential decays for multiple laser shots at a particular wavelength and then to fit the resultant decay to obtain an absorption coefficient. The correct procedure must be to fit each decay separately and average the resultant absorption coefficients.

3 Conditions for exponential decay of the light intensity

3.1 Beer-Lambert behaviour

Direct fitting of the decay of the light intensity exiting a CRDS cavity allows a constant check of the true singleexponential nature of the intensity decay. If Beer-Lambert behaviour for a single pass of the light through the cavity is violated, or if interference effects between the longitudinal and transverse modes of the cavity become pronounced, nonexponential decay can be observed and spectral intensities and absorption coefficients obtained using analysis of a single exponential will become inaccurate. Beer-Lambert behaviour requires that the widths of the absorption spectral lines are greater than the linewidth of the laser light within the cavity. This condition ensures that all of the frequencies contained within the laser pulse are attenuated by absorption when the laser is tuned to the central frequency of the absorption line. The Beer-Lambert law can only be satisfied if the pulse duration, t_p , is greater than T_2 , with T_2 , the lifetime of the upper state, determined by radiative and non-radiative decay rates. Zalicki and Zare²⁸ considered the inaccuracies in the

extracted absorption coefficients arising from different ratios of the laser linewidth to the absorption linewidth, but for our CRDS studies of predissociation on a timescale of <500 ps, this important criterion is satisfied and we expect homogeneous contributions to the linewidth of >0.01 cm $^{-1}$ and Doppler widths in the visible and UV >0.04 cm $^{-1}$.

3.2 Cavity mode effects

If the cavity is poorly designed, the frequency spacing of the longitudinal modes of the cavity (the cavity free spectral range, FSR) might exceed the widths of the spectral features being studied. Under these circumstances, light of the appropriate frequency for excitation of certain spectral lines will not be injected into the cavity and the absorption features will be absent from the resultant spectrum.²⁹ Similarly, if the bandwidth of the probe laser is narrower than the cavity mode spacing, as the external laser wavelength is scanned, the cavity response will show a series of spikes at the frequencies of the cavity modes.

A number of authors have considered the implications of cavity mode structure on the applicability of CRDS for determining accurate absorption coefficients and for recording complete spectra. ^{28–31} Both time and frequency domain treatments have been employed, and the two methods are linked by the Fourier transform. The exponential decay of light within the cavity can be shown to be equivalent to the cavity possessing Lorentzian longitudinal cavity modes, and the frequency spacing of these cavity modes, Δv , depends on the round-trip time, t_r , of light within the cavity (and hence the separation of the cavity mirrors, l) according to:

$$\Delta v = \frac{1}{t_r} = \frac{c}{2l} \tag{5}$$

Thus for the 1.5 m cavity used in our experiments, the longitudinal mode spacing for the TEM_{00} transverse mode is 100 MHz (0.003 cm⁻¹), as shown in Fig. 4. The sharpness of these cavity modes and the contrast of the transmittivity of the cavity for frequencies at and between the mode maxima depends on the mirror reflectivity and hence the decay time. For experiments in which the laser light pulse is not carefully tailored to match the TEM₀₀ mode of the cavity, or is not injected perfectly axially into the cavity, transverse cavity modes will be established that have frequencies lying between those of the longitudinal cavity modes. As discussed by Lehmann and Romanini²⁹ and Hodges et al.,³⁰ even in the impulsive limit of a laser pulse having a duration shorter than the cavity round-trip time (so that the front end of the pulse does not overlap the rear end propagating in the same direction) the frequency components of the pulse within the cavity must still match cavity mode frequencies for transmission into and through the cavity. Provided the bandwidth of the light injected into the cavity spans several cavity modes,

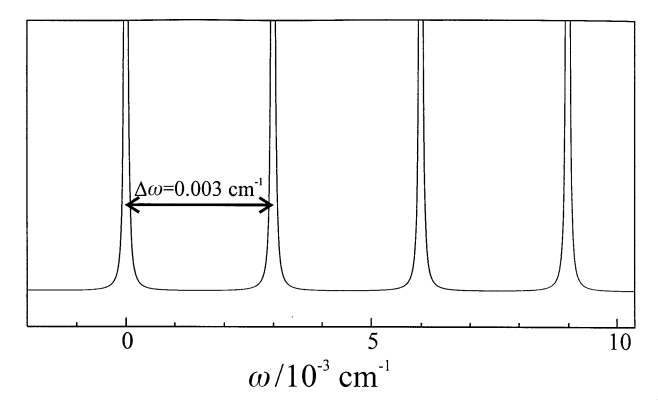


Fig. 4 Calculated longitudinal mode structure of a 1.5 m long cavity

however, the probe laser can be scanned continuously and give a ring-down intensity at all nominal laser wavelengths. In practice, the frequency restrictions imposed by cavity longitudinal modes are considerably relaxed by transverse mode structure and by cavity instabilities, so that the frequencies supported by a cavity are essentially continuous. If the coherence length of the laser pulse is less than the round-trip time within the cavity, the laser bandwidth will exceed the cavity longitudinal mode spacing. A dye laser bandwidth of ca. 0.05 cm⁻¹ means that in our 1.5 m cavity at least 15 cavity longitudinal modes are spanned for each dye laser wavelength setting. For higher-resolution lasers, such as cw seeded pulseamplified dye lasers and optical parametric oscillators (OPOs), or cw ring dye lasers, however, a careful consideration of the effects of cavity modes becomes more critical. Molecular absorption features must also overlap one or more cavity modes to contribute to the decay of light within the cavity (i.e. to feature in the recorded spectrum).

Excitation of a single, Lorentzian cavity mode will result in exponential decay of the light intensity within the cavity. The effect of exciting numerous cavity modes is to give a multiple exponential decay unless the different modes have the same losses per round trip. Even in this instance, beating between the different frequency components can result in a modulation of the exponential decay. In addition, for a cavity excited on numerous transverse cavity modes, the light emitted from the cavity can experience temporal interference because of beating between the slightly different decay rates of the separate TEM_{mn} modes. This mode beating can lead to nonexponential decays, and oscillatory structure superimposed on the decay envelope, as demonstrated by Martin et al. 35 for the excitation of a 50 cm cavity using transform-limited pulses from an IR OPO. The laser pulses had a coherence time and pulse duration greater than the round-trip cavity time, and the resultant decays show severe oscillations in amplitude. Generally, however, this mode beating is much faster than the decay time of the exponential and hence can be filtered electronically or averaged out in the fitting.

Under most circumstances, the amplitude of oscillations caused by mode beating is small compared with the decay trace of interest, however, and the exponential decay rate can be extracted by fitting the decay envelope. Collection of the entire cross-section of the beam at the detector is important to suppress transverse mode beating effects. Transverse modes can also be suppressed either by spatially matching the input laser beam to the TEM₀₀ mode of the cavity or by placing apertures in the cavity. If the mirror coatings are not of uniform reflectivity across the different profiles of the different transverse cavity modes, multiple-exponential decays can arise as a result of different losses for the different modes.

A final potential pitfall that merits mention here is the coherent interaction of molecules with the recurring laser pulse if the lifetime of the excited molecular state (with dephasing time T_2) exceeds the cavity round-trip time. This regime of timescales has been discussed at length elsewhere. For the studies of predissociation described in this article, the lifetimes of the upper state are typically less than 500 ps and we need not concern ourselves with the effect of recurrent pulses within the cavity. Note that if $T_2 < t_r$ the absorption feature will span many cavity modes, and similarly for $T_2 < t_p$, the requirement that the laser bandwidth is narrower than the absorption feature will be satisfied for transform limited pulses.

The general conclusion of detailed considerations of the possible causes of spectral inaccuracies in CRDS, however, is that in the bulk of experiments performed to date, cavity mode effects have not significantly distorted the measured spectra. The method is most prone to mode effects when either the absorption lines are very sharp or the bandwidth of the laser is comparable to or less than the free spectral range of the cavity.

4 Sensitivity of CRDS

A primary application of CRDS is in the non-invasive detection of trace species, whether in the laboratory, as has already been demonstrated for static samples and for hostile environments, such as plasmas and flames, or, as will surely be demonstrated soon, in field measurements of the atmosphere. For direct spectroscopic detection of trace species which might be present at the parts per million (ppm) or parts per billion (ppb) level, extreme sensitivity is clearly essential and several recent CRDS studies have shown that the technique can be used to monitor certain species at these very low concentrations. 33,36,37 For example, Romanini *et al.* 38 cite a detection limit of 10^{-9} cm $^{-1}$ or 5×10^{-8} per pass for the fourth C—H stretching overtone of C_2H_2 at wavelengths around 570 nm detected using a ring dye laser.

The fractional loss of intensity per round trip, $\delta I = (I_0 - I)/I_0$, is commonly used to specify the sensitivity of CRDS. For a single pass through a cavity of length l, the Beer-Lambert law gives the absorption as

$$I = I_0 \exp\{-\alpha l\} \tag{6}$$

and for very small absorbances in a single pass ($\alpha l \ll 1$), we can approximate

$$\delta I = \frac{I_0 - I}{I_0} \approx \alpha l \tag{7}$$

This equation can also be written in terms of the change in decay rate of the ring-down signal, $\Delta k = 1/\tau' - 1/\tau$, as:

$$\delta I = \Delta k \, \frac{l}{c} \tag{8}$$

Zalicki and Zare²⁸ show that for a change in the ring-down time $\Delta \tau = \tau - \tau'$ upon tuning to an absorption feature, the corresponding absorbance per pass is

$$\alpha l = (1 - R) \frac{\Delta \tau}{\tau'} \tag{9}$$

Hence the minimum detectable fractional absorption per pass (or absorbance per pass) can be written as

$$\delta I_{\rm m} \approx (1 - R) \frac{\Delta \tau_{\rm min}}{\tau} = (1 - R) \frac{\Delta N_{\rm min}}{N}$$
 (10)

where $\Delta \tau_{\min}$ is the minimum detectable change in ring-down time on absorption (*i.e.* the precision of $\Delta \tau$). The equation has also been written in terms of the number of round trips in the cavity, N, and the accuracy to which this number can be measured, ΔN_{\min} .

As an illustration, suppose a 1 m cavity is bounded by mirrors of reflectivity R=0.9999, so that the 1/e ring-down time is ca. 30 μ s. If the minimum detectable change in the ring-down time is 6.7 ns, corresponding to measuring the number of round trips of the light pulse (which should be ca. 4500) to an accuracy of within one round trip (i.e. $\Delta \tau_{\min}=6.7$ ns, or $\Delta N_{\min}=1$), then the minimum fractional absorption per pass is $\delta I_{\min}=2\times 10^{-8}$, or 20 ppb. We could also express this sensitivity in terms of a minimum absorption coefficient $\alpha_{\min}=2\times 10^{-10}$ cm⁻¹ for l=100 cm using eqn. (7).

The shortcomings of other methods of specifying the sensitivity have been described in detail by Scherer $et~al.^{32}$ The sensitivity of the method depends on the accuracy to which the ring-down time can be measured and as the ring-down time increases because of increasing mirror reflectivity, the accuracy to which $\Delta \tau/\tau$ can be determined also increases. Hence, Scherer $et~al.^{32}$ advocate specifying the mirror reflectivity when the sensitivity of an experiment is quoted. The sensitivity will reduce as the strength of absorption increases because the ring-down time decreases on a strong absorption. Other factors influencing the detection sensitivity (and degrad-

ing it from the above described optimum sensitivity) include the noise introduced by the laser and detector (including shot noise) and the resolution of the detection electronics (for example an 8-bit digitizer has a vertical resolution of 1 part in 256 whereas for a 12-bit digitizer, 1 part in 4096 resolution is possible for each laser shot). The effects of shot noise have been discussed by Scherer *et al.*³² and are considered by these authors to be small compared to the effects described above. Sensitivity can also be degraded by amplified spontaneous emission (ASE) in the laser beam. Romanini and Lehmann³³ describe an ASE filter used to suppress this contamination of the laser pulse but for most modern dye lasers, ASE contributes only a very small percentage of the laser intensity.

5 Applications of CRDS

5.1 Diagnostics

Given the foregoing description highlighting the generality and sensitivity of the CRDS technique, and its potential as a means of providing quantitative column densities, it is inevitable that it will find use as a new laser-based diagnostic technique in a whole range of analytic applications. Indeed, the first illustration was reported in the seminal paper of O'Keefe and Deacon¹ with their demonstration of O₂ detection in air, with a fractional absorbance per pass of ca. 1 ppm, whilst follow up work demonstrated 1 ppb detectivity for NO_2 . 36 As well as atmospheric monitoring, these workers also foresaw the applicability of CRDS as a means of probing chemical processes in hostile environments (e.g. flames, plasmas and discharges). Not surprisingly, given its widespread importance, OH was amongst the first radical species to be detected by CRDS, on its A-X transition in the near UV, both in a Bunsen flame³⁹ and simply in a heated (1000 °C) sample of air.40 Scherer et al.41 have extended these studies into the IR (to ca. 3 µm, so as to cover the O-H stretching fundamental) and obtained OH column densities as a function of height for the flame atop a McKenna-type plug burner. The same group has also used CRDS for HCO radical detection (on its predissociated, visible A-X band system) in a low-pressure CH₄-N₂-O₂ flame, ⁴² and demonstrated the determination of absolute HCO concentrations of ca. 2×10^{13} cm⁻³, in good accord with predictions of flame chemistry simulations. They estimated a limiting detection sensitivity for this species, by CRDS at 300 K, that is competitive with all existing techniques, including intracavity laser absorption spectroscopy.

Arguably the most impressive application yet reported of CRDS as a diagnostic technique is the work on methyl radical detection by the Stanford group. 43-45 The CH₃ radical is widely held to be the key growth species in the chemical vapour deposition of polycrystalline diamond films in low power reactors;46,47 thus any rational attempt at process optimisation will require knowledge of absolute methyl radical number densities, [CH₃], their spatial variation within the reactor and their dependence on process conditions. The Stanford group chose to monitor CH3 radicals via the predissociated B-X system around 213.9 nm, for which both the absolute absorption cross-section and its temperature dependence are reasonably well documented, 48 and to use a hot filament reactor. This reactor comprised a five-way stainlesssteel cross (two arms of which are extended to form the ring down cavity), and contained a resistively heated filament and an independently heated Mo strip substrate positioned ca. 7 mm distant (on which diamond CVD occurs), through which the process gas mixture (0.5% CH₄ in H₂, 100 sccm flow rate, 20 Torr pressure) is passed. The entire reactor is designed to be translated relative to the fixed laser probe beam (propagating parallel to the long axis of the filament) to enable spatially resolved profiling of the methyl radical number densities. The power of the technique is illustrated in Fig. 5 which shows absorbances measured as a function of

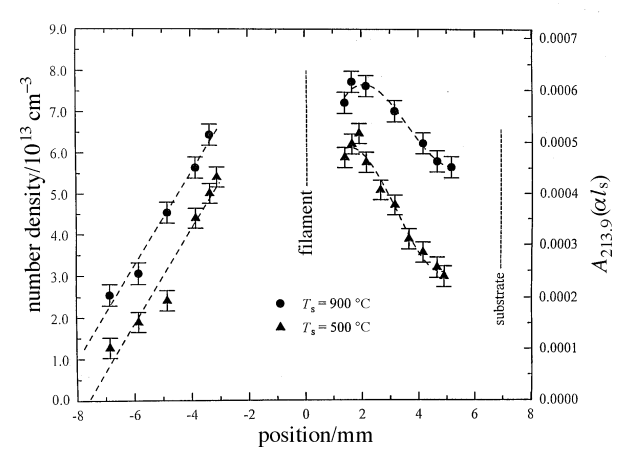


Fig. 5 Spatial profiles of the ${\rm CH_3}$ number density (absorbance) within a hot-filament reactor at two different substrate temperatures. The ${\rm CH_3}$ was detected by CRDS at a wavelength of 213.9 nm. The filament temperature was 2300 K, the total pressure was 20 Torr, and a gas mixture of 0.5% ${\rm CH_4}$ in ${\rm H_2}$ flowed from left to right at a rate of 100 sccm. Figure reproduced from ref. 45 with permission.

distance from the hot filament, moving both towards (right hand panel) and away from (left hand panel) the substrate, for two different substrate temperatures. The measured absorbances can be converted into [CH₃], provided one makes an assumption about the column length over which radicals are formed, here assumed to be simply the length of the filament.

Key findings include the following:

- (i) The actual magnitudes of [CH₃], which accord well with values derived *via* molecular beam mass spectrometric (MBMS) probing of similar hot filament reactors, ^{49,50} but are some 10–100 times larger than those estimated by REMPI probing.⁵¹
- (ii) The spatial dependence of [CH₃] which, because it peaks away from the filament, strongly suggests that gas phase chemistry (rather than, e.g. surface-catalysed decomposition on the filament) is the main CH₃ radical production route,
- (iii) (Not shown.) The increase in [CH₃] that accompanies increase in the temperature of either the filament or substrate.

There can be little doubt that CRDS will find increasing use as a diagnostic technique. The technique is ripe for many atmospheric applications, e.g. monitoring O₃ in the UV or, possibly, in the IR, species like O₂, NO₂ and NO₃ in the visible, HO₂ and other small peroxyl radicals via their structured electronic band systems in the near IR (as an alternative to probing their UV absorption systems which are all continuous and rather similar), and a wide range of hydrides (both stable molecules and radical species) via their vibrational fundamental or overtone transitions where species selectivity is likely to be greatest.

5.2 Reaction kinetics

Lin and co-workers first applied CRDS to the study of rates of chemical reactions using laser pump and probe techniques, with the traditional probe methods such as LIF or laser absorption replaced by CRDS detection. They performed extensive studies of the reactions of the phenyl radical with species such as O_2 , CCl₄, Cycloalkanes, and HBr. Ammundation at the second relied on detection either of C_6H_5 at 504.8 nm or $C_6H_5O_2$, formed by adding small amounts of O_2 to the reaction mixture, at 496.4 nm. The same group has since studied the reaction of NH₂ with NO by photolysing NH₃ at 193 nm in the presence of NO and monitoring the loss of absorption by NH₂ at 537.6 nm. Since Studies of the study of the stud

Atkinson and Hudgens⁶² compared measurements of the rates of reaction of $C_2H_5 + C_2H_5$, $C_2H_5O_2 + C_2H_5O_2$, and $O_2 + C_2H_5 + Ar$ using CRDS detection with rates deter-

mined by alternative methods and found good agreement, thereby demonstrating the validity of CRDS as a tool for measurement of reaction rate coefficients. These experiments used 308 nm excimer laser photolysis of Cl₂ to initiate a sequence of reactions in a mixture of Cl₂, ethane, O₂ and argon, with Cl-atom abstraction of H from C₂H₆, forming C₂H₅. A combination of a cylindrical lens and a beam mask in the path of the photolysis laser provided a well-defined pathlength over which the CRDS detection of reactive species occurred. More recently, these same workers⁶³ have determined the rate of self reaction of the propargyl radical (CH₂CCH), formed by 193 nm photolysis of methyl acetylene.

As an illustration of the application of CRDS to determine rate coefficients, however, we use recent work from Hudgens and co-workers⁶⁴ on the reactions of IO, which are of current interest as a better understanding of the role of IO in the chemistry of the atmosphere is sought. IO was formed in a flow tube *via* a sequence of steps initiated by 193 nm laser photolysis of N₂O:

$$N_2O + hv(193 \text{ nm}) \rightarrow N_2 + O(^1D)$$

 $O(^1D) + M \rightarrow O(^3P) + M$
 $O(^3P) + CF_3I \rightarrow IO + CF_3$.

where M is a collisional quencher, e.g. Ar.

IO can be detected via the A $^{2}\Pi$ -X $^{2}\Pi$ transition at ca. 450 nm using CRDS. The mirrors employed in the study gave a ring-down time of ca. 1 µs: this short RDT compared with many of the experiments described in this article means a reduced sensitivity, but ensures that the timescale of the measurement of [IO] is short compared with the time delay between photolysis and probe laser pulses. Thus, the concentration of IO does not vary significantly over the timescale of the CRDS measurement. A spectrum of the (2, 0) band of IO is shown in Fig. 6. For a mixture of N₂O-CF₃I-NO-Ar, the variation in IO signal at the (2, 0) bandhead ($\lambda = 445$ nm) with increasing delay between the photolysis laser and a probe laser is illustrated in Fig. 7, with the absorption plotted in ppm as described in Section 4. Under the experimental conditions, IO is formed on a timescale of ca. 100 µs, and the subsequent decay is caused by loss of IO, primarily through reaction with NO. Modelling of the decay under pseudo-firstorder conditions gives a rate coefficient for the IO + NO reaction of 1.85×10^{-11} cm³ molecule⁻¹ s⁻¹, in excellent agreement with previous (non-CRDS) studies.⁶⁵

5.3 Molecular spectroscopy

CRDS has been applied to a variety of molecular spectroscopic applications, a selection of which we now summarise briefly.

5.3.1 Vibrational spectroscopy. High vibrational excitation of molecules may be used to characterise the topology of ground state potential-energy surfaces in regions energetically distant from the bottom of the potential well. Information can also be obtained about intramolecular energy flow and the possible evolution from regular to chaotic energy level structure. High-overtone transitions are inherently weak, however, and therefore require very sensitive probe techniques. Photoacoustic spectroscopy has, until recently, been the probe method of choice, but CRDS also has sufficient sensitivity and has the distinct advantage of being a direct absorption technique allowing quantitative studies of transition intensities. We have recorded CRDS and photoacoustic spectra of the fourth C-H stretching overtones of C2H2 and C2HD and observe similar signal-to-noise ratios for similar pressures of the gases in the two experiments. The validity of an absolute comparison of the relative sensitivities is not well addressed by

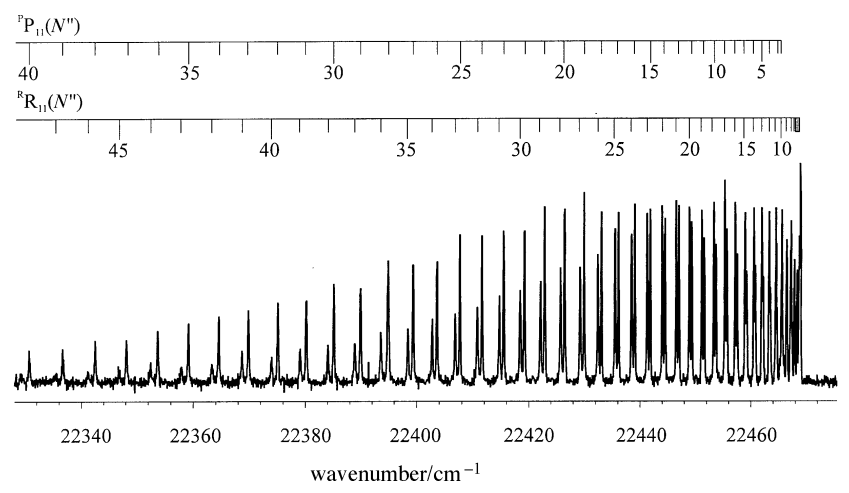


Fig. 6 CRD spectrum of the IO A ${}^2\Pi_{3/2}$ –X ${}^2\Pi_{3/2}$ (2, 0) band. The rotational line assignments are shown by the combs above the spectrum.

our experiments since in neither case did we try hard to optimise the signal-to-noise ratio. We note, however, that for the CRDS detection, much lower laser intensities are required, and because only a very small percentage of the laser intensity enters the ring-down cavity, power broadening effects evident in the photoacoustic spectrum are entirely absent in the CRD spectrum.

The observed line positions and intensities for overtone spectra are strongly dependent on the shape of the portion of the potential energy surface probed and may be compared with theoretical values obtained using *ab initio* or empirically determined potentials in order to test and further refine these potentials. Romanini and Lehmann^{33,66} have used CRDS to extend the range of observed overtones in HCN up to six, seven and eight stretching quanta for various isotopomers, and compared their observed spectroscopic frequencies and constants with those derived from various calculated potential energy surfaces. They found only a few perturbed bands despite the very high vibrational excitation.

CRDS is now being extended to the spectroscopy of the fundamental vibrations of molecules lying in the IR region of the spectrum. Scherer *et al.*³⁷ observed the IR-active v_3 mode of CH₄ *via* its fundamental transition, and Saykally and coworkers have reported IR CRDS spectra of $(H_2O)_n$, n = 1-6, clusters.⁶⁷⁻⁶⁹

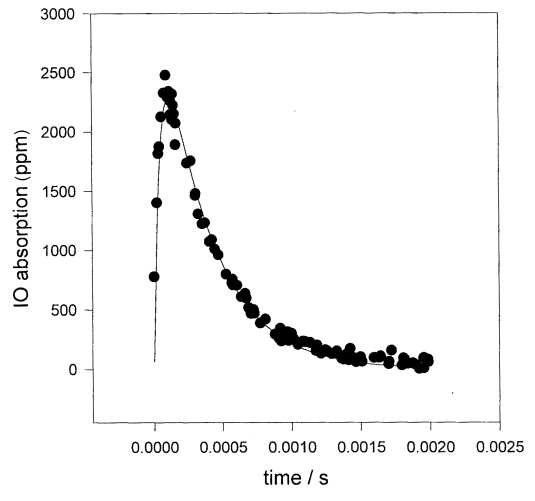


Fig. 7 Variation of the IO absorbance with time delay between photolysis and probe lasers for a mixture of CF_3I , N_2O , NO, and argon. The solid circles are experimental data points and the line is a fit to the data. 193 nm photolysis of N_2O generates oxygen atoms that react with CF_3I to form IO, giving the observed rise in the CRDS signal. The subsequent decay is caused by the reaction of IO with NO and a fit to the decay rate yields a rate constant for the reaction.

5.3.2 Electronic spectroscopy. The exceptional sensitivity of CRDS makes it ideally suited to the investigation of weak molecular transitions or of molecules present at low concentrations, and the technique has the added advantage of providing quantitative spectral intensities. These features have been exploited in studies of electronic transitions of a range of gas-phase molecules; some are detailed here whilst others are discussed more extensively in Section 6.

Slanger and co-workers 70,71 observed and characterized five new bands of the O_2 Herzberg system in the $40\,950-41\,300\,\mathrm{cm^{-1}}$ region, namely the (12, 0) and (13, 0) bands of the $A'\,^3\Delta_u-X\,^3\Sigma_g^-$ transition, the $c\,^1\Sigma_u^--X\,^3\Sigma_g^-$ (17, 0) and (18, 0) bands, and the $A\,^3\Sigma_u^+-X\,^3\Sigma_g^-$ (12, 0) band, and were able to determine improved spectroscopic constants. Engeln *et al.* ⁷² demonstrated the utility of phase shift CRDS by obtaining a spectrum of the very weak $b\,^1\Sigma_g^+-X\,^3\Sigma_g^-$ (2, 0) band of $^{18}O_2$. A combination of CRDS with a hollow cathode discharge enabled Maier and co-workers to observe the N_2^+ $A\,^2\Pi_u-X\,^2\Sigma_g^+$ (6, 0) band 73 and a $^2\Pi-X\,^2\Pi$ transition of C_6H (and C_6D). 74 The C_6H radical is of interest in radioastronomy, and pairs of bands due to the $^2\Pi_{1/2}-X\,^2\Pi_{1/2}$ and $^2\Pi_{3/2}-X\,^2\Pi_{3/2}$ components were identified. Band origins were accurately determined, improving on values from previous matrix-isolation studies. Lehr and Hering 75 recently made comparisons of the linear CRDS and non-linear DFWM techniques using the spectrum of NaH as a test case. They reported sensitivities of 10^9 molecules cm $^{-3}$ per quantum state.

CRDS offers an ideal approach to studying electronic spectroscopy of small and even medium-sized cluster systems where rapid internal conversion and predissociation processes often occur upon excitation. Saykally and co-workers have, to date, applied CRDS spectroscopy to a variety of bare metal dimers and trimers, such as Cu₂, Cu₃, ⁷⁶ and Al₂, ⁷⁷ and metal silicides, such as CuSi, ⁷⁸ AgSi, ⁷⁹ AuSi, ⁸⁰ and PtSi, ⁸¹ using a novel, long pathlength, pulsed slit-valve apparatus. This area of research using CRDS has been reviewed extensively elsewhere, ^{32,82,83} and will not be discussed any further here.

The study of predissociation of excited electronic states has been our primary application of CRDS to date, and in the following Section we describe recent results for a number of molecules and radicals.

6 Predissociation dynamics

Excitation of a molecule to a bound state which is coupled to a dissociative continuum gives rise to a phenomenon known as predissociation since the excited-state molecules can fragment at energies lower than the dissociation limit of the bound state. The absorption linewidth of a transition to a predissociative level is usually broadened as a consequence of the upper state lifetime being short compared to a non-

predissociative level. The fragmentation of the excited species $AB^*(v, J)$ can be represented as:

$$AB + hv \longrightarrow AB^*(v, J) \xrightarrow{k_{\text{pre}}} A + B \quad \text{predissociation}$$

$$\xrightarrow{k_{\text{rad}}} AB(v', J') + hv'$$

fluorescence

The natural (observed) lifetime of $AB^*(v, J)$ is dependent upon the relative magnitudes of the rates of two competing processes, the radiative decay rate (fluorescence to lower states) and the predissociation rate:

$$\frac{1}{\tau} = \frac{1}{\tau_{\text{rad}}} + \frac{1}{\tau_{\text{pre}}} \tag{11}$$

If $k_{\rm pre} \gg k_{\rm rad}$ then the quantum yield for fluorescence is very small and little or no LIF signal is observed. LIF is thus generally restricted to studies of relatively slow predissociations that occur on a timescale comparable to that of radiative decay. Given its sensitivity, CRDS is ideally suited to the study of rapid predissociation of small radicals and reactive molecules even if they can only be generated at low concentrations. This is because CRDS is a linear absorption technique and, for sufficiently fast predissociation processes, the line broadening due to predissociation is large enough that the contribution to the spectral lineshape from lifetime broadening may be easily deconvoluted from the contributions from Doppler shifts, the laser bandwidth, and other broadening mechanisms. The lifetime of the state, τ , can then be related to the FWHM of the Lorentzian component of the lineshape $via:^{84}$

$$\Gamma/\text{cm}^{-1} = \frac{1}{2\pi c\tau} \tag{12}$$

For example, a 5 ps lifetime corresponds to a linewidth of 1.06 cm⁻¹. A detailed study of predissociation that measures both the vibrational and rotational dependence of the predissociative lifetime offers a valuable approach to explore state-selected unimolecular chemical reaction dynamics on coupled potential energy surfaces. This is the primary application of CRDS that we have pursued thus far in Bristol. We have used CRDS to investigate predissociation effects in a variety of diatomic and triatomic species. Some of these molecules and radicals are of importance in determining the chemistry of the Earth's atmosphere, the atmospheres of other planets in the solar system, and other astrophysical environments. Thus, the

detection of these molecules by CRDS not only enables a more detailed understanding of their photochemistry and the evolution of their electronically excited states, but also demonstrates the viability of CRDS for studying the reactions of these species. In this Section, we summarise some of our recent results to illustrate the implementation of the CRDS technique.

6.1 SH/SD A $^2\Sigma^+$

The A $^{2}\Sigma^{+}$ states of SH and SD are extensively predissociated, with only the v'=0 levels showing LIF spectra. A careful, high-resolution LIF spectrum of the SH A $^{2}\Sigma^{+}$ -X $^{2}\Pi$ (0, 0) band in a molecular beam⁸⁵ revealed lifetime broadening of spectral lines and the natural lifetime was shown to decrease monotonically with the rotational quantum number N' from 3.2 ns (N'=0) to 0.95 ns (N'=9), in good agreement with earlier studies using fluorescence quenching. Kawasaki et al.86 measured fluorescence lifetimes of SD A $^2\Sigma^+$ v' = 0 N' = 0–13 and also observed a monotonic decrease in lifetime with increasing N' from 198 to 44 ns. However, the only previous observation of higher vibrational levels (v' > 0) comes from absorption studies by Ramsay and co-worker87 using a grating spectrograph. The A-X (1, 0) band of SH was observed to be diffuse and the linewidth for individual rotational lines was estimated to be 0.1 cm⁻¹ corresponding to a lifetime of 50 ps.

Using the technique of CRDS we have recorded spectra of the A $^2\Sigma^+$ -X $^2\Pi$ (1, 0) band of SH (see Fig. 8) and the (1, 0) and (2, 0) bands of SD. 26,88 SH was produced continuously in a flow discharge apparatus coupled to our CRD spectrometer via the reaction H + H₂S \rightarrow SH + H₂. SD was produced by the analogous reaction of D atoms with D₂S. These production methods also caused some S₂ contamination of the spectra. From the spectra we have accurately determined the lifetimes of SH A $^2\Sigma^+$ v'=1 and SD A $^2\Sigma^+$ v'=1, 2 by measuring the lifetime-dependent Lorentzian broadening of individual spectral lines. The results of these measurements along with earlier work for SH and SD A $^2\Sigma^+$ v'=0 are summarised in Table 1.

The $A^2\Sigma^+$ state of SH is crossed by three repulsive states, as shown in Fig. 9. The primary coupling mechanism to the repulsive states is spin-orbit coupling. In order to rationalise the CRDS and earlier LIF data and thus elucidate information about the mechanism of the predissociation, a theoretical model employing an accurate, experimentally determined, $A^2\Sigma^+$ state potential and *ab initio* repulsive potentials and spin-orbit coupling matrix elements⁸⁹ was used to perform

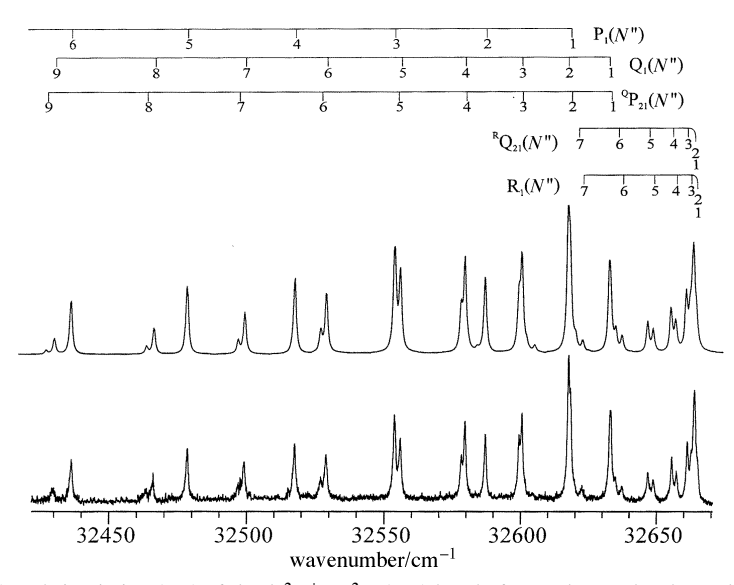


Fig. 8 CRD spectrum (bottom) and simulation (top) of the A $^2\Sigma^+$ -X $^2\Pi$ (1, 0) band of SH. The combs above the spectra indicate rotational line assignments. The simulation includes a Lorentzian component to the rotational linewidths of 1 cm⁻¹ because of lifetime broadening.

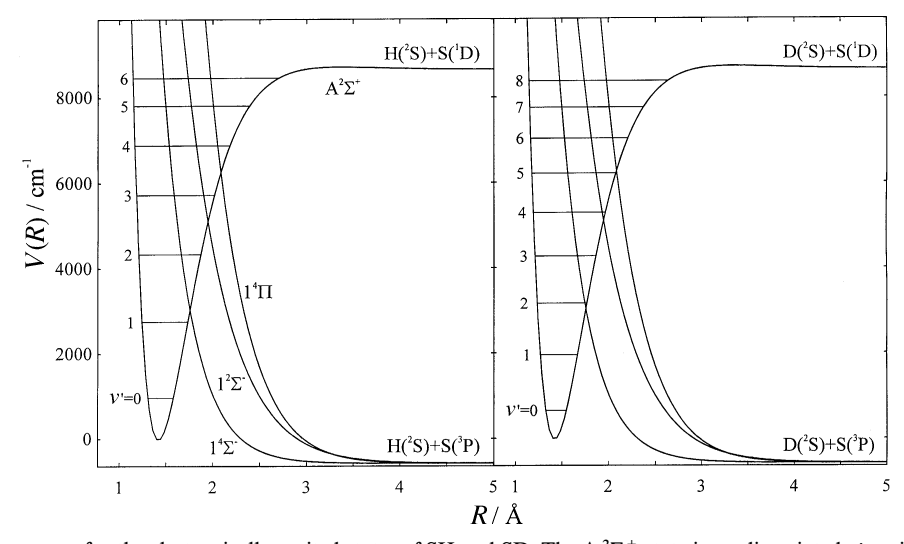


Fig. 9 Potential energy curves for the electronically excited states of SH and SD. The A $^2\Sigma^+$ state is predissociated *via* spin-orbit coupling to the $1^4\Sigma^-$, $1^2\Sigma^-$ and $1^4\Sigma$ states. The proximity of the vibrational energy levels of the A state to the crossing points of the bound and repulsive curves strongly influences the predissociation rate.

Table 1 Summary of the variation of SH/SD A $^2\Sigma^+$ v' lifetimes for experimentally observed levels typically over the range $N' \approx 0$ –10

	lifetime	lifetime	
v'	SH	SD	
0 1 2	3.20–0.95 ns ^a 5.45–4.61 ps	247–38 ns ^b 35–24 ps 2.31 ps	

Fermi Golden Rule calculations. ⁹⁰ Fig. 10 shows the results of our experimentally determined lifetimes compared with the theoretical predictions for the v'=1 level of SH(A $^2\Sigma^+$). As can be seen, there is not only extraordinarily close agreement between the absolute lifetimes predicted by the model calculations and our experimental observations but the calculations also reproduce the form of the N' dependence. The model also quantitatively reproduces the observed predissociation rates for SH A $^2\Sigma^+$ v'=0 and for SD A $^2\Sigma^+$ v'=0, 1, and 2. We observe that the primary predissociation route for the lowlying vibrational levels of the A state is via the $1^4\Sigma^-$ state, although our calculations suggest that predissociation by the $1^2\Sigma^-$ and $1^4\Pi$ states becomes significant for higher v'.

There are many parallels between the predissociation of SH A $^2\Sigma^+$ and OH A $^2\Sigma^+$, since the latter is also crossed by $^4\Sigma^-$,

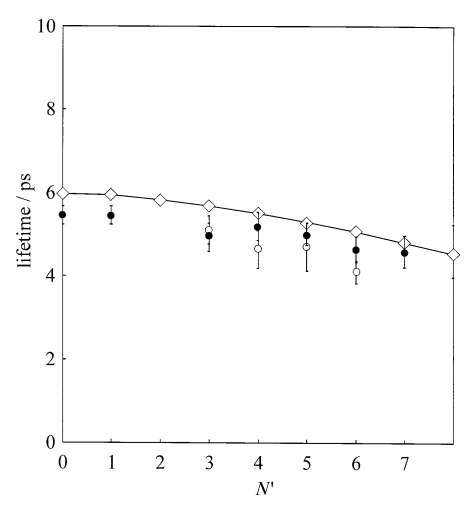


Fig. 10 Variation of the lifetimes of SH A $^2\Sigma^+$ v'=1, N' levels with N' for *e*-parity (\bigcirc) and f-parity (\bigcirc) levels. (\diamondsuit) Lifetimes of the levels calculated using a model that is summarized in the text.

 $^2\Sigma^-$, and $^4\Pi$ repulsive states which interact with the A $^2\Sigma^+$ state via spin–orbit coupling. 91 For OH, however, this spin–orbit coupling is weaker than for SH and thus observed predissociation rates are slower for the lighter radical. Hence, OH A $^2\Sigma^+$ shows a more extensive LIF spectrum than SH A $^2\Sigma^+$ and a recent comparison of CRDS and LIF spectral line intensities for the OH A $^2\Sigma^+$ –X $^2\Pi$ (3, 0) transition confirmed earlier studies of the N' dependence of the v'=3 predissociation. 92

6.2 BrO A ²Π

BrO is formed in the upper atmosphere following UV photolysis of bromine-containing compounds such as halons. Once formed in the stratosphere BrO can engage in catalytic destruction of ozone and is implicated in the chemistry leading to the formation of the springtime Antarctic ozone hole. 93

BrO has an inverted $^2\Pi$ ground state with a spin-orbit splitting constant of -976 cm $^{-1}$. The A $^2\Pi_{3/2}$ –X $^2\Pi_{3/2}$ band system has been well characterised via more traditional flash-photolysis and UV absorption techniques. 94,95 Most of the observed vibrational bands are unstructured though a few show some very diffuse rotational structure indicating a v'-dependent predissociation. Any spectroscopic investigation of BrO is hampered by the almost equal natural abundances of the two isotopes of Br (50.69% 79 Br: 49.31% 81 Br) thus greatly increasing spectral congestion.

Using CRDS we have demonstrated a laser-based detection scheme for the A ${}^{2}\Pi_{3/2}$ -X ${}^{2}\Pi_{3/2}$ band system of BrO, with the BrO produced via either of the reactions, $Br + O_3 \rightarrow BrO$ $+ O_2$ or $O + Br_2 \rightarrow BrO + Br$. The Br or O atoms are produced by passing Br2 or O2, diluted in Ar, through a microwave discharge. In these experiments, the estimated upper limit for the concentration of BrO is 5×10^{12} molecule cm⁻³. A spectrum of the A ${}^2\Pi_{3/2}$ -X ${}^2\Pi_{3/2}$ (7, 0) band is shown in Fig. 11 together with a 300 K simulation using spectroscopic constants for the ground state⁹⁴ and refined A-state constants. These constants were obtained by simulating the band contours of both 79BrO and 81BrO simultaneously and performing a least-squares fit in which the band origins, rotational constants, and Lorentzian linewidth were floated. The linewidths determined in this way are 3.2 cm⁻¹; our fitting procedure does not allow for possible J dependence of the predissociation rate. The (12, 0) band also shows rotational structure, and we determine a rotational linewidth for transitions to v' = 12 of 4 cm⁻¹. These results imply predissociation on timescales of ca. 1.3-1.6 ps.

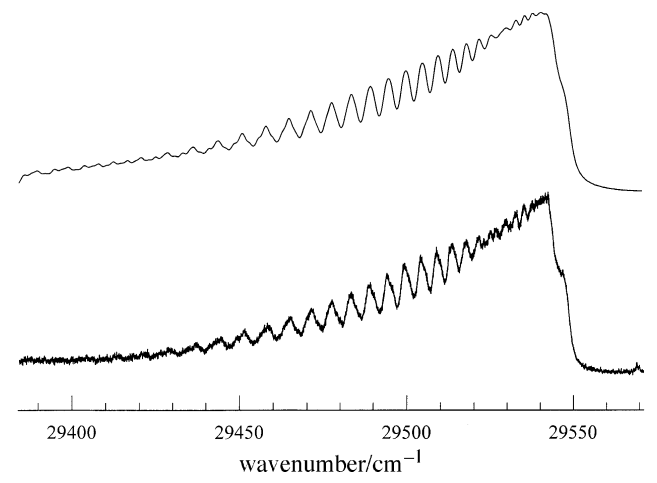


Fig. 11 CRD spectrum of the BrO A $^2\Pi_{3/2}$ -X $^2\Pi_{3/2}$ (7, 0) band, together with a spectral simulation (above). The simulation includes both isotopes of Br in their appropriate natural abundances and a rotational linewidth of 3.2 cm $^{-1}$ to account for lifetime broadening. The tail of the band corresponds to transitions between levels with rotational quantum numbers of $N \approx 30$ -40.

LIF is inappropriate for studies of the kinetics of reactions of BrO since the rapid predissociation of all levels of the A state precludes fluorescence. Our demonstration of the simplicity of detecting BrO with high sensitivity *via* CRDS should enable further studies of the rates of reaction of BrO to be performed using this spectroscopic probe. Related studies on the kinetics of the IO radical using CRDS detection on the A–X (2, 0) band were described earlier (Section 5.2).⁶⁴

6.3 $S_2 B^3 \Sigma_u^-$

The UV $B^3\Sigma_u^--X^3\Sigma_g^-$ band system of S_2 has recently received renewed interest because of its observation after the collision of comet Shoemaker–Levy 9 with Jupiter. The band system is highly complex and exhibits many perturbations which have led to difficulties in spectral analysis. The $B^3\Sigma_u^--X^3\Sigma_g^-$ transition was studied extensively by Green and Western 56,97 for levels with v'<10 using LIF of S_2 in a molecular beam and these authors presented a deperturbation model to explain the observed behaviour in terms of mixing between the $B^3\Sigma_u^-$ and $B''^3\Pi_u$ states, which are shown schematically in Fig. 12. Levels of the $B^3\Sigma_u^-$ state with $v'\geqslant 10$ lie above the dissociation limit for the B'' and X states: hence the fluorescence lifetime is greatly reduced owing to the onset of predissociation. The primary cause of the predissociation is

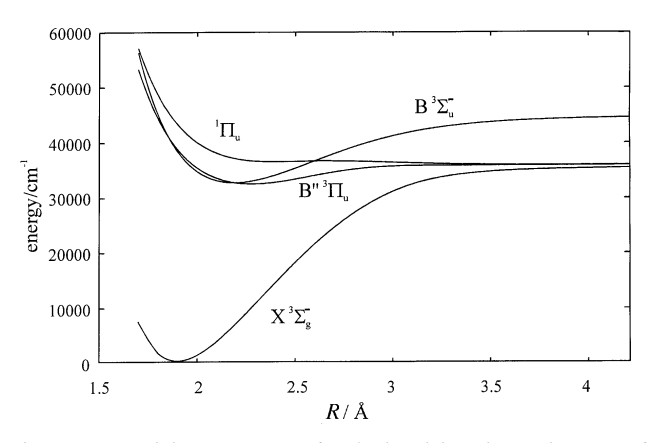


Fig. 12 Potential energy curves for the low-lying electronic states of S_2 involved in the predissociation of the $B\,^3\Sigma_u^-$ state. The potential for the B state is an RKR potential derived from spectroscopic determination of vibrational band origins for the $B\,^3\Sigma_u^-$ -X $^3\Sigma_g^-$ transition. The other potentials were calculated using *ab initio* techniques.

thought to be a repulsive $^1\Pi_{\rm u}$ state crossing the outer limb of the B state.

We have recently recorded spectra of the B ${}^{3}\Sigma_{u}^{-}$ -X ${}^{3}\Sigma_{g}^{-}$ (v', 0) bands for v' = 10-22 using our CRDS apparatus.⁹⁸ The S₂ was produced in continuous flow by the reaction of hydrogen atoms with H₂S. Fig. 13 shows a spectrum of the S₂ B-X (16, 0) band together with a simulation. Spectral analysis reveals not only improved values for rotational constants and band origins, but also a linewidth that varies substantially over the range of vibrational levels explored. The improved and extended band origin values have permitted the construction of an RKR potential for the B state. To simulate the band contours, we require linewidths that range from 6 to ca. 20 cm⁻¹ depending on the upper vibrational level. We also note that the variation of the linewidth and hence predissociation rate does not change monotonically with v', but rather that the bands appear to become continuous and then structured once more before becoming totally diffuse at v' = 18. These results are consistent with earlier, qualitative observations of line broadening using a grating spectrometer⁹⁹ and imply that more than one repulsive state causes the predissociation. We are currently conducting ab initio electronic structure calculations and Fermi Golden Rule calculations of the rates of predissociation to identify the state(s) responsible for the predissociation and clarify the fragmentation mechanism.

6.4 HNO Ã ¹A"

The HNO molecule is of particular interest in the field of molecular dynamics, both for its complicated predissociation behaviour and for the comparisons that can be drawn between it and the HCO and HO₂ radicals. Above its groundstate dissociation limit, HCO exhibits extensive, sharp vibrational structure corresponding to long-lived vibrational modes (primarily C=O stretches) embedded in the continuum of $\rm H + CO.^{100}$ On the other hand, $\rm HO_2$ shows no such structure, but is better described by irregular (statistical) dynamical behaviour in this regime. 101 HNO might be expected to show intermediate behaviour, with evidence of some vibrational structure above the ground-state dissociation limit. In our laboratory, 102 an investigation of several vibrational bands (v_1, v_2, v_3) $(v_1$ is the N-H stretch, v_2 the N=O stretch, and v_3 the H-N=O bend) of the \tilde{A} $^1A''-\tilde{X}^{-1}A'$ transition and their underlying K' sub-structure has been carried out using CRDS. The spectra reveal perturbations of the A-state levels and, for excitation to levels of the A-state lying above the dissociation limit, show J'-dependent line broadening occurring within several of the bands. This latter observation indicates a rotationally induced predissociation mechanism.

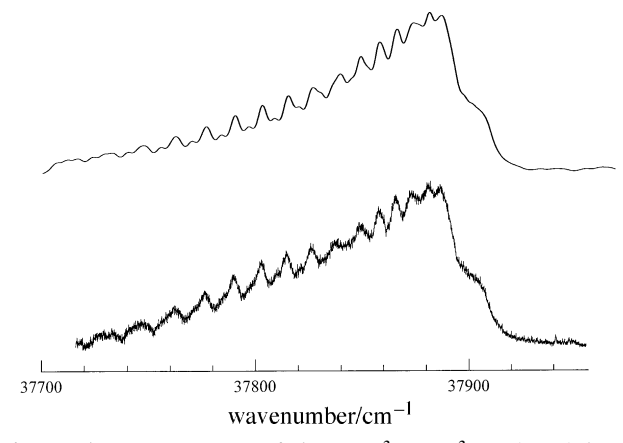


Fig. 13 A CRD spectrum of the S_2 B $^3\Sigma_u^-$ -X $^3\Sigma_g^-$ (16, 0) band. Shown above the experimental spectrum is a simulation that includes a Lorentzian component of the rotational linewidths of 6 cm⁻¹. The tail of the band corresponds to transitions between levels with rotational quantum numbers of $N'' \approx 40$.

HNO was made in continuous flow by the three-body reaction $H + NO + M \rightarrow HNO + M$ with the H atoms produced by passing a microwave discharge through H₂. A typical CRD spectrum of part of the $\tilde{A}^{1}A''-\tilde{X}^{1}A'$ (100–000) and (020– 000) bands together with an LIF spectrum of the same region is shown in Fig. 14. This figure shows clearly the fluorescence signal deteriorating rapidly due to the onset of predissociation at high J' levels in both bands, whereas the CRD spectrum shows many lifetime-broadened levels above the predissociation threshold. J'-dependent lifetime broadened linewidths have been measured for transitions to various upper state levels and the broadening varies from 0.01 to 0.3 cm⁻¹. In order to explain the linewidth dependences on rotation and vibration a model has been proposed in which levels of the excited state predissociate via a doorway state which is itself coupled to the continuum. Possible candidates for these doorway states are quasi-bound vibrational levels of the $\tilde{X}^{1}A'$ state (cf. HCO) or vibrational levels of the \tilde{a}^3A'' state. A number of considerations support the former candidate.

- 1. A higher density of states within the $\tilde{X}^{1}A'$ state manifold.
- 2. The linewidths increase with K' consistent with a type-a electronic-rotational Coriolis coupling between the $\tilde{\mathbf{A}}$ and $\tilde{\mathbf{X}}$ states.
- 3. K' = 0 levels predissociate more slowly than levels with K' > 0, due to *b*-axis Coriolis coupling being intrinsically weaker than *a*-axis coupling.
- 4. Predissociation is more rapid upon excitation of the bending mode which enhances Renner-Teller coupling between the \widetilde{A} and \widetilde{X} states.

The J' dependence may then arise from energy-tuning between stacks of levels in both the \tilde{A} and \tilde{X} states. Likely doorway states have been investigated using the potential energy surfaces (PESs) of Guadagnini $et\ al.^{103}$ and these calculations suggest that vibrational levels of the \tilde{X} state lying above the dissociation limit that involve excitation of the N=O stretch, such as the (0, 13, 0) level, are only weakly coupled to the H+NO continuum. Our data also suggest, however, that for the \tilde{A}^1A'' (110) state, the onset of predissociation to the continuum of the \tilde{a}^3A'' state is observed. This suggestion is supported by calculations using the abovementioned PESs that locate the \tilde{A}^1A'' (110) level energetically close to the top of the barrier on the \tilde{a}^3A'' state.

To complement our work on HNO, we investigated isotopic effects on the dynamics and spectroscopy of the $\tilde{A}^{1}A''$ state by recording CRD spectra of DNO above the dissociation threshold. Dixon and Rosser¹⁰⁵ measured a J'-dependent breaking-off in fluorescence in a total of six

sub-bands within three vibronic transitions (020)–(000), (021)–(000), and (110)–(000). By extrapolation to J'=0 they determined a limiting curve for predissociation with limit of $17\,030\pm10$ cm⁻¹. There is no observable line-broadening in any of our spectra suggesting that the coupling between the $\tilde{A}^{1}A''$ and $\tilde{X}^{1}A'$ states is much weaker than for HNO. This observation is entirely consistent with the predissociation model proposed for HNO, since the second-order *a*-axis Coriolis coupling is proportional to the square of the *a*-axis rotational constant.

7 Recent developments in CRDS methods

The majority of applications of CRDS to date have made use of high-powered pulsed lasers of the type used in the experiments performed at Bristol and described in Section 2. The multi-mode structure of these laser pulses and their bandwidths of >0.04 cm⁻¹ mean that careful frequency matching of the cavity to the laser pulse is not necessary since the laser bandwidth spans numerous cavity mode frequencies. Recent extensions of the CRDS method include the use of transform limited pulses and continuous wave lasers, including compact, low power diode lasers, as higher resolution and smaller instrumentation is sought in CRD spectroscopy. In principle, the resolution of a CRDS experiment will be limited not by the laser bandwidth but by the width of the cavity longitudinal modes, which for the very high finesse cavities used in CRDS can be sharper than the laser bandwidth even for highresolution lasers.²⁹ For cw applications, where the bandwidth of the laser is likely to be less than the free spectral range of the cavity, two techniques have been developed for matching the laser frequency to cavity modes so that the laser wavelength and absorption spectrum can be scanned continuously. Engeln et al.72 used an intensity-modulated cw laser and measured the spectrum from the wavelength dependent phase shift of the light exiting the cavity. Rather than actively lock the cavity length to the wavelength of the laser to ensure continuous scanning, the cavity was designed to have a very dense mode structure so that the narrowband cw laser was coupled into the cavity for a fraction of a microsecond every 10 or so microseconds because of slight thermal drifts in cavity length, mechanical instability, etc. Romanini and co-workers have demonstrated cw CRDS using both a cw ring dye laser (probing an acetylene overtone at 570 nm)³⁸ and an external cavity diode laser. 106,107 One cavity-end mirror was mounted on a piezo-electric transducer. The input laser beam was mode matched to the cavity TEM₀₀ mode using two lenses and a

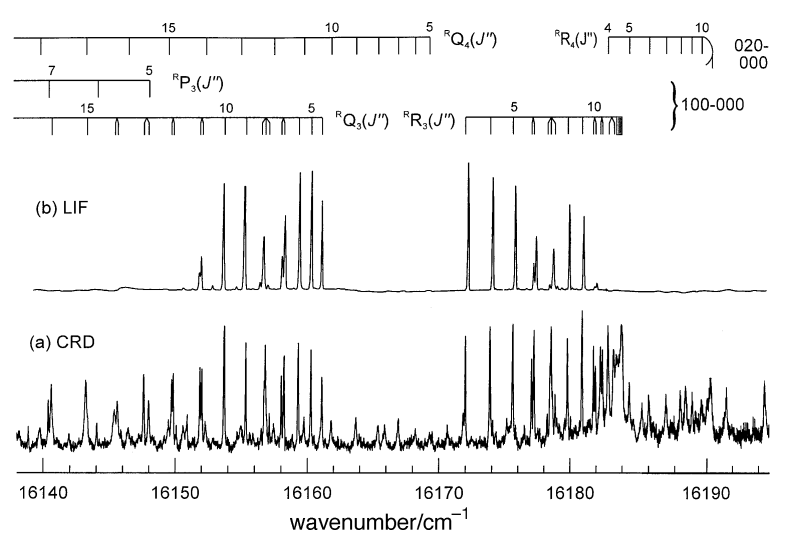


Fig. 14 LIF (top) and CRD (bottom) spectra of the HNO $\tilde{A}^1A''-\tilde{X}^1A'$ transition (100)–(000) K'=4-K''=3 and (020)–(000) K'=5-K''=4 sub-bands. Line assignments are shown by the combs above the spectra. Much of the structure present in the CRDS spectrum is absent in the LIF spectrum because of predissociation of the \tilde{A} state.

spatial filter, and the cavity length was modulated using the piezo-electric transducer so that the frequency of one longitudinal mode oscillated around the laser frequency. Each time the mode frequency passed through the laser frequency, light was coupled into the cavity and a ring-down event could be observed if the laser was then interrupted using an acousto-optic modulator (AOM). The demonstrated sensitivity of 5×10^{-8} per pass is comparable to pulsed CRDS. Paldus *et al.* ¹⁰⁸ have also successfully performed diode-laser CRDS experiments and used an AOM to modify the bandwidth of the diode laser *via* feedback to the laser cavity. The prospects of constructing a compact instrument using diode-laser based CRDS apparatus for trace gas detection either in the laboratory or in the field, in for example atmospheric monitoring, seem close to becoming a reality.

At the other extreme of resolution, Meijer and coworkers^{109,110} have recently combined broadband CRDS with spectral resolution of the light exiting the cavity using an FT spectrometer. The ca. 10 cm⁻¹ bandwidth pulses at wavelengths around 10–11 μ m were generated using a free electron laser and absorption of ethylene on the v_7 fundamental was used to illustrate the technique. The limitation of this approach is that the scan rate of the FT spectrometer is slower than the normal wavelength scanning speed of a higher resolution laser, but with a dispersive element such as a monochromator and a time and position sensitive detector, such as the modified CCD arrays developed by Rowley et al., 111 more rapid spectral data accumulation with broadband sources should be feasible.

Hagemeister and Zwier¹¹² have developed a hybrid LIF–CRDS technique to study clusters in supersonic jets. If the LIF is accumulated orthogonal to the cavity axis over the full ring-down time then, despite the fact that only ca. 0.1% (if $R \approx 0.999$) of the incident laser light is coupled into the RDC, the multiple passes through the sample result in an LIF spectrum of comparable quality to that obtained by a single pass of the entire laser beam through the sample. A major advantage, however, is that the CRDS-LIF spectrum is much less prone to saturation effects because of the low laser intensity in the cavity. The method has been exemplified by studies of tropolone and tropolone– $(H_2O)_n$ clusters.

In extreme contrast to all other CRDS applications performed to date, Pipino et al. 113 have proposed and developed a means of applying the method to studies of solid/gas and solid/liquid interfaces. The technique makes use of evanescent waves, much as does attenuated total internal reflection (ATR) spectroscopy, but by using a ring-down cavity, should greatly enhance the sensitivity. Two implementations have been proposed: the simpler method places a superpolished Pellin-Broca prism inside a (right-angled) traditional CRDS cavity bounded by mirrors. 114 Adsorption of I2 at one face of the prism resulted in attenuation of the light intensity within the cavity at a greater rate than the losses at the surfaces and within the prism. The second method relies on coupling of light into a monolithic cavity using the evanescent wave from a 90° prism. The monolithic cavity is a regular polygonal prism and the light propagates in a ring within the prism and is coupled out to a detector via a second, right-angled prism. This exciting idea has not yet been implemented experimentally. Engeln et al.115 recently reported that, despite 4% reflections per surface, a transparent solid sample can be placed within a cavity and induce losses of only 10^{-3} per pass provided the surface reflections are recaptured by the cavity. As an illustration of the technique, they measured the optical rotation of a 2 mm thick sample of optically flat BK7.

8 Future prospects

From the foregoing it is obvious that CRDS offers a whole range of new possibilities; it is safe to assume that there are

more, as yet unthought of, to come.

Before concluding with a paragraph summarising some real and imagined prospects for the technique it is perhaps worth commenting on its limitations, amongst the more obvious are the following.

- (i) The method samples along a column, rather than at a point, which may prove restrictive when attempting spatial profiling in very inhomogeneous environments.
- (ii) CRDS is a 'one-dimensional' technique in the sense that the only user-selectable degree of freedom is the excitation frequency. All absorbing species in the cavity will contribute to the ring down time (recall the S₂ contamination of the SH spectrum mentioned in Section 6.1). Thus sample purity may be more of an issue than for rival techniques such as LIF (where the frequency dependence of both the excitation and detection steps can be used to aid species selectivity) or REMPI, where the spectral carrier can be distinguished not just by the spectrum in frequency space but also by monitoring the mass spectrum of the resulting ions or the kinetic energy distribution of the accompanying photoelectrons.
- (iii) The mirror reflectivity, and its constancy over a long timescale, are crucial aspects of the technique, the maintenance of which may necessitate particularly careful cavity design in cases where CRDS is to be applied to 'dirty' environments.

Nonetheless, the wavelength ranges over which the high reflectivity mirrors required for CRDS are available is steadily increasing. CRDS can now be applied for wavelengths ranging from the deep UV to the mid IR. This extension into the IR, and, in particular, to the 'fingerprint' region of molecular vibrational spectroscopy offers widespread applications for laser diagnostics, indeed, one such study has just been performed. 116 The advent of cw CRDS using solid-state diode lasers promises compact instruments for atmospheric remote sensing. A particularly favourable starting point is likely to be monitoring of the NO₃ radical, responsible for night-time tropospheric oxidation, which has strong absorptions around 662 nm and 623 nm. The use of small-volume cavities offers the prospect of spectroscopic detection and study of compounds available only in very small quantities, such as some isotopically labelled species. The possibilities have already been demonstrated by the recent study of the $b^{\,1}\Sigma_g^{\,\,+} - X^{\,3}\Sigma_g^{\,\,-}$ spectrum of ¹⁸O₂. ⁷² The development of CRDS using monolithic cavities 113 and with solid samples inside the more usual RDCs114,115 also offers the prospect of extending this technique into studies of condensed phases.

We gratefully acknowledge the many contributions to the CRDS experiments performed in Bristol by K. N. Rosser, Prof. R. N. Dixon, Dr C. M. Western, Dr J. Pearson, S. E. Johnson, C. D. Brooks, J. Spashett, and A. P. Hawkins. Valuable collaborations with Prof. M. Kawasaki and Prof. T. Ishiwata were made possible by the Japan–UK Cooperative Program of the Japanese Society for Promotion of Science, the British Council and the Royal Society. A.J.O.E. thanks the Royal Society for the award of the Eliz. Challenor Research Fellowship, M.D.W. thanks the University of Bristol for the award of a postgraduate scholarship and S.M.N. thanks NERC for a studentship. Funding for the CRDS experiments was provided by the Royal Society, NERC and EPSRC.

References

- A. O'Keefe and D. A. G. Deacon, Rev. Sci. Instrum., 1988, 59, 2544.
- 2 J. M. Herbelin, J. A. McKay, M. A. Kwok, R. H. Uenten, D. S. Urevig, D. J. Spencer and D. J. Bernard, Appl. Opt., 1980, 19, 144
- D. Z. Anderson, J. C. Frisch and C. S. Masser, *Appl. Opt.*, 1984, 23, 1238.
- 4 C. M. Western, Chem. Soc. Rev., 1995, 24, 299 and references therein.

- 5 M. N. R. Ashfold, in An Introduction to Laser Spectroscopy, ed. D. L. Andrews and A. A. Demidov, Plenum Press, New York, 1995 and references therein.
- P. F. Bernath, Spectra of Atoms and Molecules, Oxford University Press, New York, 1995.
- J. Ballard, K. Strong, J. J. Remedios, M. Page and W. B. Johnston, J. Quant. Spectrosc. Radiat. Transfer, 1994, 52, 677.
- J. Pfab, in Applied Laser Spectroscopy: Techniques, Instrumentation and Applications, ed. D. L. Andrews, VCH, New York, 1992
- D. J. Creasey, P. A. Halford-Maw, D. E. Heard, M. J. Pilling and B. J. Whitaker, J. Chem. Soc., Faraday Trans., 1997, 93, 2907; D. E. Heard and M. J. Pilling, personal communication.
- 10 K. P. Huber and G. Herzberg, Constants of Diatomic Molecules, van Nostrand Reinhold, New York, 1979.
- M. N. R. Ashfold, S. G. Clement, J. D. Howe and C. M. Western, J. Chem. Soc., Faraday Trans., 1993, 89, 1153.
- M. N. R. Ashfold and J. D. Howe, Annu. Rev. Phys. Chem., 1994, 12
- 13 M. N. R. Ashfold, Mol. Phys., 1986, 58, 1.
- W. Demtroder, Laser Spectroscopy, Springer-Verlag, Berlin, 1981.
- J. Davidson, J. H. Gutow and R. N. Zare, J. Phys. Chem., 1990, 15 94, 4069 and references therein.
- R. L. Abrams, J. F. Lam, R. L. Lind, D. G. Steel and P. F. Liao, in Optical Phase Conjugation, ed. R. L. Fischer, Academic Press, New York, 1983.
- 17 H. J. Eichler, P. Günter and D. W. Pohl, Laser Induced Dynamic Gratings, Springer-Verlag, Berlin, 1986.
- 18 R. L. Farrow and D. J. Rakestraw, Science, 1992, 257, 1894 and references therein.
- 19 M. D. Wheeler, I. R. Lambert and M. N. R. Ashfold, Chem. Phys. Lett., 1994, 229, 285.
- G. Hall and B. J. Whitaker, J. Chem. Soc., Faraday Trans., 1994, 20 90, 1.
- S. Williams, D. S. Green, S. Sethuraman and R. N. Zare, J. Am. Chem. Soc., 1992, 114, 9122.
- D. S. Green, T. G. Owano, S. Williams, D. G. Goodwin and 22 R. N. Zare, Science, 1993, 259, 1726.
- 23 A. Campargue, F. Stoeckel and M. Chenevier, Spectrochim. Acta Rev., 1990, 13, 69.
- 24 V. A. Lozovsky, S. Cheskis, A. Kachanov and F. Stoeckel, J. Chem. Phys., 1997, 106, 8384.
- J. Pearson, A. J. Orr-Ewing, M. N. R. Ashfold and R. N. Dixon, J. Chem. Phys., 1997, 106, 5850.
- M. D. Wheeler, A. J. Orr-Ewing and M. N. R. Ashfold, J. Chem. Phys., 1997, 107, 7591.
- A. Yariv, Quantum Electronics, Wiley, New York, 3rd edn., 1989. 27
- P. Zalicki and R. N. Zare, J. Chem. Phys., 1995, 102, 2708. 28 29
- K. K. Lehmann and D. Romanini, J. Chem. Phys., 1996, 105,
- 30 J. T. Hodges, J. P. Looney and R. D. van Zee, Appl. Opt., 1996, **35**, 4112.
- J. T. Hodges, J. P. Looney and R. D. van Zee, J. Chem. Phys., 31 1996, 105, 10278.
- J. J. Scherer, J. B. Paul, A. O'Keefe and R. J. Saykally, Chem. Rev., 1997, 97, 25.
- D. Romanini and K. K. Lehmann, J. Chem. Phys., 1993, 99, 33 6287
- J. W. Hudgens, personal communication.
- J. Martin, B. A. Paldus, P. Zalicki, E. H. Wahl, T. G. Owano, J. S. Harris Jr., C. H. Kruger and R. N. Zare, Chem. Phys. Lett., 1996, **258**, 63,
- A. O'Keefe and O. Lee, Am. Lab., 1989, 21, 19.
- J. J. Scherer, D. Voelkel, D. J. Rakestraw, J. B. Paul, C. P. Collier, R. J. Saykally and A. O'Keefe, Chem. Phys. Lett., 1995, 245, 273.
- 38 D. Romanini, A. A. Kachanov, N. Sadeghi and F. Stoeckel, Chem. Phys. Lett., 1997, **264**, 316.
- G. Meijer, M. G. H. Boogaarts, R. T. Jongma, D. H. Parker and A. M. Wodtke, Chem. Phys. Lett., 1994, 217, 112.
- R. T. Jongma, M. G. H. Boogaarts, I. Holleman and G. Meijer,
- Rev. Sci. Instrum., 1995, 66, 2861. J. J. Scherer, D. Voelkel and D. J. Rakestraw, Appl. Phys. B., 1997, 64, 699.
- J. J. Scherer and D. J. Rakestraw, Chem. Phys. Lett., 1997, 265, 169.
- 43 P. Zalicki, Y. Ma, R. N. Zare, E. H. Wahl, J. R. Dadamio, T. G. Owano and C. H. Kruger, Chem. Phys. Lett., 1995, 234, 269.
- P. Zalicki, Y. Ma, R. N. Zare, E. H. Wahl, T. G. Owano and C. H. Kruger, Appl. Phys. Lett., 1995, 67, 144.

- 45 E. H. Wahl, T. G. Owano, C. H. Kruger, P. Zalicki, Y. Ma and R. N. Zare, Diamond Rel. Mater., 1996, 5, 373.
- M. N. R. Ashford, P. W. May, C. A. Rego and N. M. Everitt, *Chem. Soc. Rev.*, 1994, 23, 21.
- D. G. Goodwin and J. E. Butler, in Handbook of Industrial Diamond and Diamond Films, ed. M. A. Prelas, G. Popovici and L. K. Bigelow, Marcel Dekker, in press.
- S. M. Hwang, M. J. Rabinowitz and W. C. Gardiner, Chem. Phys. Lett., 1993, 205, 157 and references therein.
- 47 W. L. Hsu, Appl. Phys. Lett., 1991, 59, 1427.
- R. S. Tsang, PhD Thesis, University of Bristol, 1997.
- N. Ota and N. Fujimori, in Advances in New Diamond Science and Technology, ed. S. Saito, N. Fujimori, O. Fukunaga, M. Kamo, K. Kobashi and M. Yoshikawa, MYU, Tokyo, 1994, p. 127.
- T. Yu and M. C. Lin, J. Am. Chem. Soc., 1993, 115, 4371.
- T. Yu, M. C. Lin and C. F. Melius, Int. J. Chem. Kinet., 1994, 26, 1095.
- T. Yu and M. C. Lin, J. Phys. Chem., 1994, 98, 2105.
- 55 T. Yu, A. M. Mebel and M. C. Lin, J. Phys. Org. Chem., 1995, 8,
- T. Yu and M. C. Lin, J. Am. Chem. Soc., 1994, 116, 9571.
- 57
- T. Yu and M. C. Lin, *J. Phys. Chem.*, 1994, **98**, 9697. T. Yu and M. C. Lin, *J. Phys. Chem.*, 1995, **99**, 8599. 58
- T. Yu and M. C. Lin, Int. J. Chem. Kinet., 1993, 25, 875.
- T. Yu and M. C. Lin, Int. J. Chem. Kinet., 1994, 26, 771.
- E. W. Diau, T. Yu, M. A. G. Wagner and M. C. Lin, J. Phys. Chem., 1994, 98, 4034.
- D. B. Atkinson and J. W. Hudgens, J. Phys. Chem. A, 1997, 101, 62 3901.
- D. B. Atkinson and J. W. Hudgens, Chem. Phys. Lett., in press.
- D. B. Atkinson, J. W. Hudgens and A. J. Orr-Ewing, in preparation.
- A. A. Turnipseed, M. K. Gilles, J. B. Burkholder and A. R. Ravishankara, Chem. Phys. Lett., 1995, 242, 427.
- D. Romanini and K. K. Lehmann, J. Chem. Phys., 1995, 102, 633.
- 67 J. J. Scherer, J. B. Paul, C. P. Collier, A. O'Keefe, D. J. Rakestraw and R. J. Saykally, Spectroscopy, 1996, 11, 46.
- J. B. Paul, J. J. Scherer, A. O'Keefe and R. J. Saykally, Laser Focus World, 1997, 33, 71.
- J. B. Paul, C. P. Collier, R. J. Saykally, J. J. Scherer and A. O'Keefe, J. Phys. Chem. A, 1997, 101, 5211.
- T. G. Slanger, D. L. Huestis, P. C. Cosby, H. Naus and G. Meijer, J. Chem. Phys., 1996, 105, 9393.
- D. L. Huestis, R. A. Copeland, K. Knutsen, T. G. Slanger, R. T. Jongma, M. G. H. Boogarts and G. Meijer, Can. J. Phys., 1994, **72**, 1109.
- 72 R. Engeln, G. von Helden, G. Berden and G. Meijer, Chem. Phys. Lett., 1996, 262, 105.
- M. Kotterer, J. Conceicao and J. P. Maier, Chem. Phys. Lett., 1996, 259, 233.
- M. Kotterer and J. P. Maier, Chem. Phys. Lett., 1997, 266, 342.
- L. Lehr and P. Hering, IEEE J. Quantum Electron., 1997, 33, 75 1465
- A. O'Keefe, J. J. Scherer, A. L. Cooksy, R. Sheeks, J. Heath and R. J. Saykally, Chem. Phys. Lett., 1990, 172, 214.
- J. J. Scherer, J. B. Paul and R. J. Saykally, Chem. Phys. Lett., 1995, **242**, 395.
- J. J. Scherer, J. B. Paul, C. P. Collier and R. J. Saykally, J. Chem. Phys., 1995, 102, 5190.
- J. J. Scherer, J. B. Paul, C. P. Collier and R. J. Saykally, J. Chem. Phys., 1995, 103, 113.
- J. J. Scherer, J. B. Paul, C. P. Collier, A. O'Keefe and R. J. Saykally, J. Chem. Phys., 1995, 103, 9187.
- J. B. Paul. J. J. Scherer, C. P. Collier and R. J. Saykally, J. Chem. Phys., 1996, 104, 2782.
- J. J. Scherer, J. B. Paul, A. O'Keefe and R. J. Saykally, Adv. Metal Semiconductor Clusters, 1995, 3, 149.
- J. B. Paul and R. J. Saykally, Anal. Chem., 1997, 69, 287A.
- H. Lefebvre-Brion and R. W. Field, Perturbations in the Spectra of Diatomic Molecules, Academic Press, New York, 1986.
- W. Ubachs, J. J. ter Meulen and A. Dymanus, Chem. Phys. Lett., 1983, 101, 1; W. Ubachs and J. J. ter Meulen, J. Chem. Phys., 1990, 92, 2121.
- M. Kawasaki, H. Sato, G. Inoue and M. Suzuki, J. Chem. Phys., 1989, 91, 6758.
- D. A. Ramsay, J. Chem. Phys., 1952, 20, 1920; J. W. C. Johns and D. A. Ramsay, Can. J. Phys., 1961, 39, 210.
- M. D. Wheeler, A. J. Orr-Ewing, M. N. R. Ashfold and T. Ishiwata, Chem. Phys. Lett., 1997, 268, 421.

- M. Riad Manaa, Int. J. Quantum Chem.; Quantum Chem. Symp., 1995. 29, 577.
- 90 R. J. LeRoy, Comp. Phys. Commun., 1989, 52, 383.
- 91 D. R. Yarkony, J. Chem. Phys., 1992, 97, 1838 and references therein
- J. J. L. Spaanjaars, J. J. ter Meulen and G. Meijer, J. Chem. Phys., 1997, 107, 2242.
- R. P. Wayne, Chemistry of Atmospheres, Clarendon Press, Oxford, 1991.
- M. Barnett, E. A. Cohen and D. H. Ramsay, Can. J. Phys., 1981, 59, 1908.
- 95 W. B. DeMore, S. P. Sander, D. M. Golden, R. F. Hampson, M. J. Kurylo, C. J. Howard, A. R. Ravishankara, C. E. Kolb and M. J. Molina, Chemical Kinetics and Photochemical Data for use in Stratospheric Modeling, Evaluation Number 11, JPL Publication 94–26, 1994.
- 96 M. E. Green and C. M. Western, J. Chem. Phys., 1996, 104, 848.
- 97 M. E. Green and C. M. Western, J. Chem. Soc., Faraday Trans., 1997, 93, 365.
- 98 M. D. Wheeler, S. M. Newman and A. J. Orr-Ewing, submitted.
- G. Herzberg, Spectra of Diatomic Molecules, van Nostrand Reinhold, New York, 1950.
- 100 C. Stock, X. N. Li, H. M. Keller, R. Schinke and F. Temps, J. Chem. Phys., 1997, 106, 5333.
- 101 M. Stumpf, A. J. Dobbyn, D. H. Mordaunt, H-M. Keller, H. Flüthmann, R. Schinke, H-J. Werner and K. Yamashita, Faraday Discuss. Chem. Soc., 1995, 102, 193.
- 102 J. Pearson, A. J. Orr-Ewing, M. N. R. Ashfold and R. N. Dixon, J. Chem. Soc., Faraday Trans., 1996, 92, 1283.

- 103 R. Guadagnini, G. C. Schatz and S. P. Walch, J. Chem. Phys., 1995, 102, 774.
- 104 R. N. Dixon, unpublished calculations.
- 105 R. N. Dixon and C. A. Rosser, Chem. Phys. Lett., 1985, 108, 323.
- 106 D. Romanini, A. A. Kachanov and F. Stoeckel, *Chem. Phys. Lett.*, 1997, 270, 538.
- 107 D. Romanini, A. A. Kachanov and F. Stoeckel, *Chem. Phys. Lett.*, 1997, 270, 546.
- 108 B. A. Paldus, J. S. Harris, J. Martin, J. Xie and R. N. Zare, J. Appl. Phys., 1997, 82, 3199.
- 109 R. Engeln and G. Meijer, Rev. Sci. Instrum., 1996, 67, 2708.
- 110 R. Engeln, E. van den Berg, G. Meijer, L. Lin, G. M. H. Knippels and A. F. G. van der Meer, Chem. Phys. Lett., 1997, 269, 293.
- 111 D. M. Rowley, M. H. Harwood, R. A. Freshwater and R. L. Jones, J. Phys. Chem., 1996, 100, 3020.
- 112 F. Hagemeister and T. S. Zwier, unpublished results.
- 113 A. C. R. Pipino, J. W. Hudgens and R. E. Huie, Rev. Sci. Instrum., 1997, 68, 2978.
- 114 A. C. R. Pipino, J. W. Hudgens and R. E. Huie, Chem. Phys. Lett., in press.
- 115 R. Engeln, G. Berden, E. van den Berg and G. Meijer, J. Chem. Phys., 1997, 107, 4458.
- 116 J. J. Scherer, K. W. Aniolek, N. P. Cernansky and D. J. Rakestraw, J. Chem. Phys., 1997, 107, 6196.

Paper 7/07686J; Received 24th October, 1997